PAPER • OPEN ACCESS

Enhanced photosensitivity in a hybrid WSe$_2$/2DEG heterojunction using a buried TiO$_2$ photosensitive layer

To cite this article: Wentai Zhu *et al* 2024 *Mater. Res. Express* **11** 056404

View the article online for updates and enhancements.

Materials Research Express

PAPER

Enhanced photosensitivity in a hybrid WSe$_2$/2DEG heterojunction using a buried TiO$_2$ photosensitive layer

Wentai Zhu[1], **Xinyue Zhang**[1], **YuanYuan Liu**[1], **Guangyao Sun**[1], **Guozhen Liu**[1], **Ju Gao**[1,2], **Zenghua Cai**[1,*], **Yucheng Jiang**[1,*] and **Run Zhao**[1,*] ᴑ

1 Jiangsu Key Laboratory of Micro and Nano Heat Fluid Flow Technology and Energy Application, School of Physical Science and Technology, Suzhou University of Science and Technology, Suzhou, 215009, People's Republic of China
2 School for Optoelectronic Engineering, Zaozhuang University, Zaozhuang 277160, People's Republic of China
* Authors to whom any correspondence should be addressed.

E-mail: zhcai@usts.edu.cn, jyc@usts.edu.cn and zr@usts.edu.cn

Abstract

In this study, we integrated the wide-bandgap material TiO$_2$ as a photosensitive layer with the WSe$_2$/2DEG heterostructure, creating a hybrid WSe$_2$/TiO$_2$/2DEG heterojunction. This hybrid structure significantly improves the device's photosensitivity, exhibiting a high rectification effect and a switching ratio of 10^3. The photodetector shows excellent performance, with a responsivity of 0.61 A W^{-1} and a detectivity of up to 1.1×10^{11} Jones at 405 nm, along with a very fast photoresponse speed. The buried TiO$_2$ channel allows photogenerated electrons to easily flow through the reduced barrier at the depleted region. This hybrid heterojunction holds promise for the development of high-performance photoelectric devices.

1. Introduction

Over the past decade, researchers have made significant breakthroughs in the study of two-dimensional (2D) materials, propelling this field to the forefront of materials science [1, 2]. Since the discovery of graphene in 2004, the family of 2D materials has grown to include graphene, black phosphorus, transition metal dichalcogenides (TMDs), and others [3–5]. TMDs, in particular, have been found to exhibit excellent optical properties, offering extensive potential for applications in optoelectronics and optical devices [6, 7]. Photodetectors are among the devices derived from TMDs that convert light signals into electrical signals, finding widespread use in communication, imaging, security, and scientific research. These 2D-based photodetectors can achieve high sensitivity across a broad wavelength range while providing fast response times, low power consumption, high integration, and flexibility, making them a major focus of current optoelectronics research [4, 8, 9]. For example, a wide-bandgap WS$_2$/Ge heterojunction photodetector demonstrates a high responsivity of 634.5 mA W^{-1} and a detectivity of up to 4.3×10^{11} Jones, with a response ranging from deep ultraviolet (200 nm) to mid-wave infrared (4.6 μm) at room temperature [10].

As research progresses, the heterostructures of two-dimensional materials, held together by van der Waals forces, have led to a range of intriguing phenomena and promising application opportunities. By skillfully combining different two-dimensional materials, it's possible to manipulate electronic structures, optical properties, and magnetic characteristics, resulting in a variety of novel properties that are hard to achieve with traditional materials [11, 12]. Additionally, stacking in the vertical direction can be accomplished through various preparation methods without the need for lattice matching. In the realm of photodetectors, a 2D stacking system with a wide bandgap and a p-n heterostructure can lead to high photoelectric performance in devices. For instance, a high photoresponsivity (3 A W^{-1}) has been observed in the vertical WSe$_2$/WS$_2$ heterostructure [13]. Besides, a novel planar 2D heterojunction consisted of 2D TMDs and two-dimensional electron gas (2DEG) represents the perfect rectifying behavior and novel physical properties [14–16]. However, the typical planar WSe$_2$/2DEG heterojunction exhibits a persistent photoconductivity characteristic, which allows the existence of charge carriers with infinite lifespan at specific transition temperatures, achieving
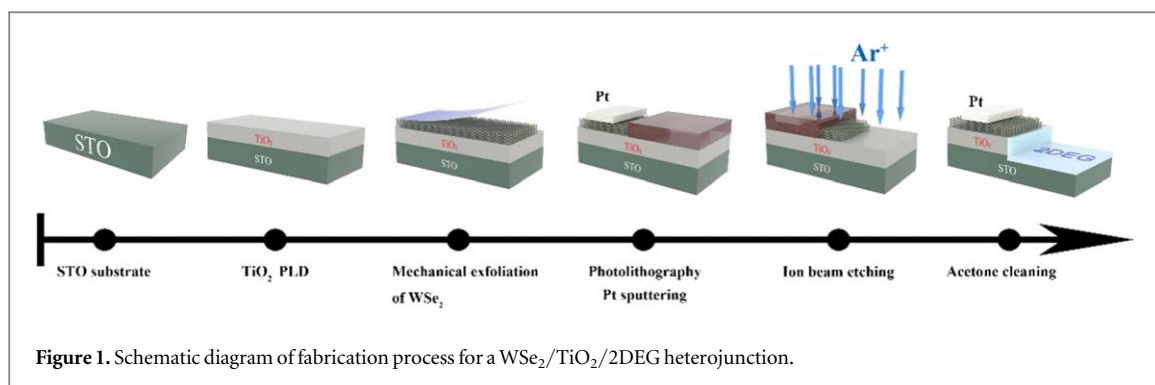
Figure 1. Schematic diagram of fabrication process for a WSe$_2$/TiO$_2$/2DEG heterojunction.

photoconversion and storage rather than photoinduction in the device [14]. Returned to that band alignment in the depleted region, the p–n interface owns a large barrier and intrinsic unique intrinsic space charge region, which cause the existence of infinite-lifetime photocarriers. Therefore, we want to realize transient photoconductivity for the purpose of high photosensitive detection, we can adjust the heterogeneous structure and introduce a wide bandgap photosensitive layer in the vertical direction to achieve the purpose [17, 18].

In this study, we designed and fabricated a hybrid heterojunction of WSe$_2$/TiO$_2$/2DEG to enhance photoconductivity. In this heterostructure, the horizontal p–n junction is composed of 2D p-WSe$_2$ and n-2DEG, while the vertical stack consists of a TiO$_2$ film and a p–n junction interface. By introducing the wide-bandgap TiO$_2$ photosensitive layer, we improved the light absorption and emission characteristics of the device due to its excellent transparency and refractive index. Additionally, with an appropriate barrier structure, we optimized the transport performance and photoresponse in the heterojunction. Experimental results show that, with the buried TiO$_2$ photosensitive layer, the device exhibits transient photoconductivity, with a response rate of 600 mA W^{-1} and a detectivity of 1.1×10^{11} Jones, along with an ultra-fast response speed. The photodetector demonstrates broad-spectrum photoresponse from ultraviolet to infrared light at room temperature, with optimal response at a 405 nm wavelength. Moreover, its self-driven feature and low turn-on voltage contribute to ultralow power consumption, making it ideal for various applications. This study provides a novel approach for designing and enhancing high-performance photodetectors for future use.

2. Methods

The fabrication process for WSe$_2$/TiO$_2$/2DEG hybrid devices involves several techniques, including Pulsed Laser Deposition (PLD), Mechanical Exfoliation, Photolithography, and Magnetron Sputtering, as depicted in figure 1. The first step is depositing an epitaxial TiO$_2$ film with a thickness of 50 nm onto a (001)-oriented STO substrate using PLD. The deposition temperature and oxygen pressure are set at 680 °C and 13 Pa, respectively, with an excimer laser operating at a frequency of 3 Hz and a laser power of 1.5 J cm^{-2}. Next, WSe$_2$ flakes are mechanically exfoliated from a bulk crystal and transferred onto the newly deposited TiO$_2$ film. Afterward, metallic platinum (Pt) electrodes are sputtered onto the WSe$_2$ flakes following photolithography. Ar^{+} ion bombardment is then applied to the other end of the WSe$_2$, creating another conductive 2DEG electrode [19]. Finally, the remaining photoresist is dissolved and removed in acetone. This process results in the successful fabrication of a hybrid heterojunction of WSe$_2$/2DEG with a buried TiO$_2$ layer.

X-ray Diffraction (XRD) was performed using a Bruker D8 diffractometer to analyze the crystal structure and orientation of the TiO$_2$ film, scanning across a θ–2θ range from 20° to 80°. The device's planar configuration was visualized through metallographic microscopy with an OLYMPUS BX51, and the film's thickness was measured with an Atomic Force Microscope (AFM, Bruker Multimode 8). To examine the transport properties of the hybrid heterojunction, the electrodes at both ends (one with a Pt electrode and the other with 2DEG) were individually connected to electrical test platforms using a wedge bonder. Photoelectrical measurements were performed with a Keithley 6517b high-resistance meter. Laser sources with wavelengths ranging from 405 to 808 nm were used to measure photoresponse.

3. Results and discussion

X-ray diffraction (XRD) was conducted to confirm the structure of the TiO$_2$ epitaxial films. Figure 2(a) shows distinct diffraction peaks in the θ–2θ scan corresponding to TiO$_2$ (002) and substrate STO(00 l) ($l = 1,2,3$). No other impurity peaks were observed, confirming a high-quality, epitaxial-oriented rutile-phase TiO$_2$ on the STO substrate [20]. The planar morphology of this hybrid heterostructure is displayed in figure 2(b), revealing a well-
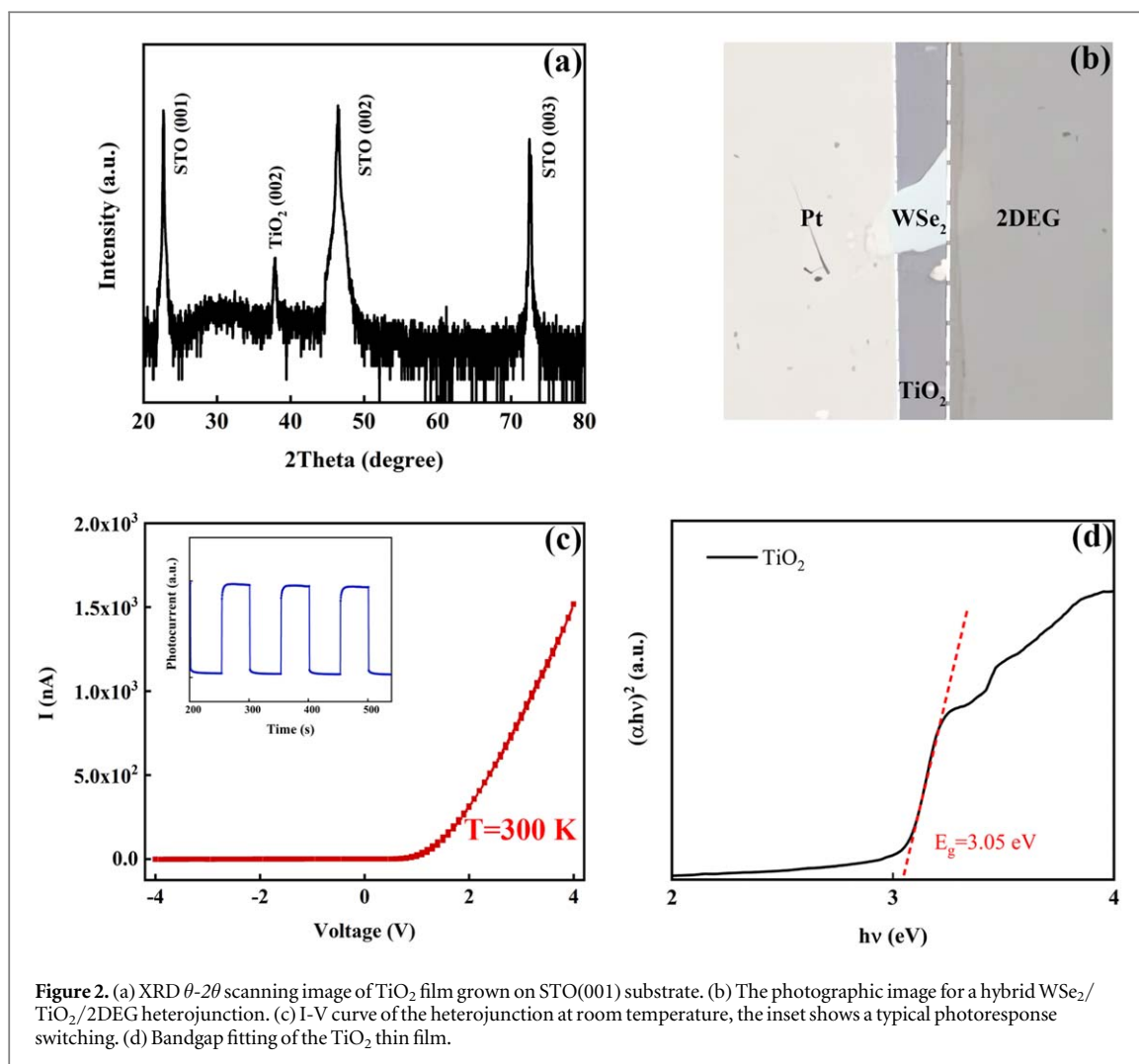
Figure 2. (a) XRD θ-2θ scanning image of TiO$_2$ film grown on STO(001) substrate. (b) The photographic image for a hybrid WSe$_2$/TiO$_2$/2DEG heterojunction. (c) I-V curve of the heterojunction at room temperature, the inset shows a typical photoresponse switching. (d) Bandgap fitting of the TiO$_2$ thin film.

defined interface without diffusion. The parallel dashed lines represent two isolated and sharp interfaces of Pt/WSe$_2$ and WSe$_2$/2DEG. Consequently, Pt, WSe$_2$, and 2DEG are connected in series and placed horizontally on the buried TiO$_2$ film. The thicknesses of the WSe$_2$ flakes, TiO$_2$ film, and etched depth are 30, 50, and 70 nm, respectively (not shown). Figure 2(c) depicts a current–voltage (I-V) curve for the WSe$_2$/TiO$_2$/2DEG heterojunction under ±4 V bias, demonstrating excellent rectification at room temperature, with a maximum photocurrent in the microampere range under forward bias and no current under reverse bias. The inset in figure 2(c) illustrates the photoresponse of the hybrid heterojunction under light illumination at room temperature, showing consistent on/off switching.

Figure 3(a) shows typical diode behavior from the dark I-V characteristics, with a consistent threshold voltage at different biases. Note that the formation of the p–WSe$_2$/n-2DEG heterojunction in our devices results in good rectification. Throughout the entire bias range, the dark leakage current at reverse bias is approximately in the picoampere range, making it negligible. However, the dark leakage current in forward bias increases with voltage, leading to a decrease in the rectification ratio under higher bias conditions [21]. The optimal rectification ratio can reach nearly 10^3 at a bias of $+4$ V (as indicated in table 1), which is used for subsequent photoresponse measurements. To understand the significant role of the wide-bandgap TiO$_2$ photosensitive layer in device performance, a systematic study on the enhanced photoconductivity was conducted in this hybrid heterojunction. During the measurement, samples were illuminated with light sources of different wavelengths, ensuring the same number of photons was used by calculating and controlling various power densities. Figure 3(b) shows the I-V curves of a hybrid WSe$_2$/TiO$_2$/2DEG heterojunction under different wavelengths at room temperature, all demonstrating a typical rectification effect with visible light. Specifically, the highest photocurrent (around mA) and the lowest turn-on voltage ($+0.6$ V) were observed with 405 nm light. The inset reveals that the maximum photocurrent at the same bias is inversely proportional to wavelength, owing to complete absorption within the visible light spectrum in the buried TiO$_2$ layer [22].

To study the photoresponse of the heterojunction at room temperature, we examined the switching performance of the hybrid heterojunction under different lighting conditions. We analyzed the relationship
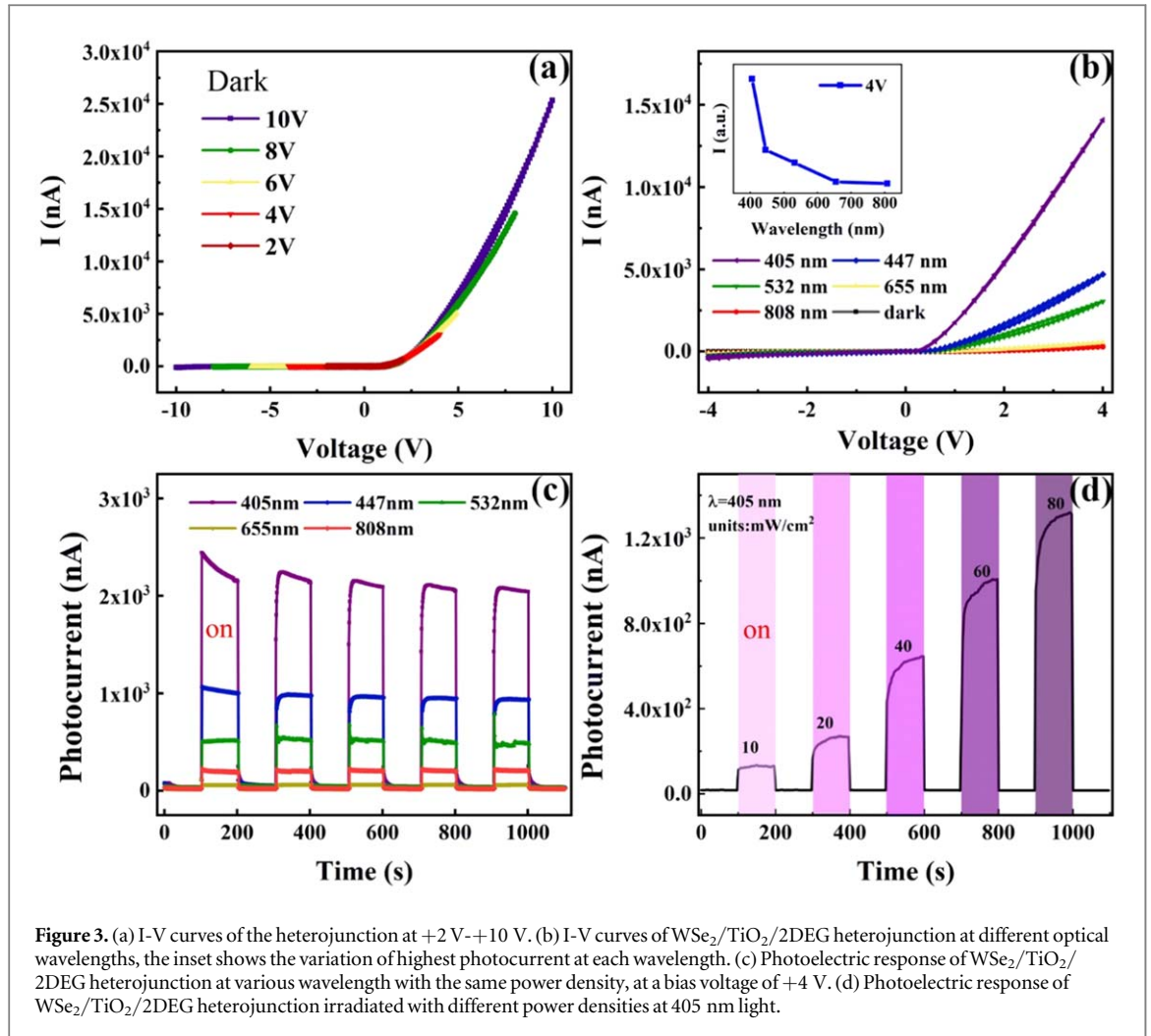
Figure 3. (a) I-V curves of the heterojunction at +2 V-+10 V. (b) I-V curves of $WSe_2/TiO_2/2DEG$ heterojunction at different optical wavelengths, the inset shows the variation of highest photocurrent at each wavelength. (c) Photoelectric response of $WSe_2/TiO_2/2DEG$ heterojunction at various wavelength with the same power density, at a bias voltage of +4 V. (d) Photoelectric response of $WSe_2/TiO_2/2DEG$ heterojunction irradiated with different power densities at 405 nm light.

Table 1. Rectification ratio of heterojunction at a range of 2 V-10 V.

Bias/V	2	4	6	8	10
Rectification ratio	452	1090	541	483	217

Table 2. The switching ratio of heterojunction under different wavelengths of light.

Wavelength/nm	405	447	532	655	808
Switching ratio	105	50	20	3.5	11

between photoresponse and wavelength by using a uniform light power density of 100 mW cm^{-2} with a light ON/OFF interval of 100 s. Across the entire optical wavelength spectrum, the photocurrents increased quickly into a conductive state when exposed to light and reverted to the initial insulative state after the light was blocked, as shown in figure 3(c). The ON/OFF switching ratio, which is detailed in table 2, strengthened as the wavelength decreased, consistent with the earlier results showing maximum photocurrent. Additionally, the optimal switching performance at 405 nm light is due to the suitable bandgap (3.0 eV, rutile TiO_2) [23]. The photoresponse in this hybrid heterojunction is 2–3 times higher than in planar $WSe_2/2DEG$ heterojunction, attributed to the added TiO_2 layer with a wider bandgap [24]. Subsequently, the 405 nm laser, which is the most responsive, was used with varying power densities to study power density-dependent switching performance, as shown in figure 3(d). As the power density increased, both the photocurrent and the ON/OFF ratio grew larger, driven by the increased generation of photogenerated carriers at higher light intensity [25]. This, combined with the previous results, indicates that introducing an epitaxial TiO_2 film as a wide-bandgap photosensitive layer
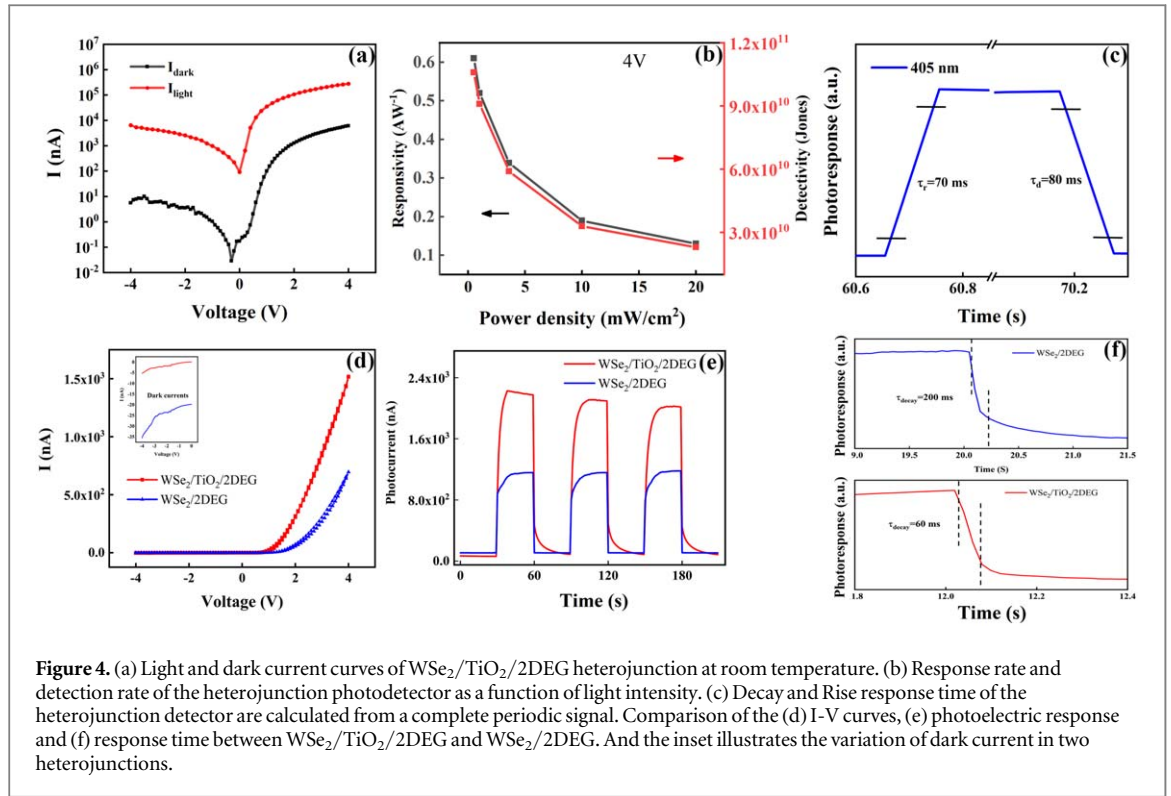
Figure 4. (a) Light and dark current curves of WSe$_2$/TiO$_2$/2DEG heterojunction at room temperature. (b) Response rate and detection rate of the heterojunction photodetector as a function of light intensity. (c) Decay and Rise response time of the heterojunction detector are calculated from a complete periodic signal. Comparison of the (d) I-V curves, (e) photoelectric response and (f) response time between WSe$_2$/TiO$_2$/2DEG and WSe$_2$/2DEG. And the inset illustrates the variation of dark current in two heterojunctions.

enhances the device's transparency and refractive index across the spectral range while optimizing light absorption and photocarrier emission in the heterojunction photodetector. Moreover, the buried layer can improve transport behavior and reduce leakage current in the heterojunction by forming a suitable barrier structure, as discussed later.

To understand the fundamental properties of a WSe$_2$/2DEG heterojunction with a wide-bandgap photosensitive layer, we conducted a series of measurements and calculations to evaluate key detector parameters such as dark current, photocurrent, responsivity (R), and detectivity (D^*) at room temperature. Using a 405 nm light with a power intensity of 3.6 mW cm^{-2}, the dark and light I-V curves of the WSe$_2$/TiO$_2$/2DEG heterojunction detector are compared in figure 4(a). Rectification behavior is observed with and without illumination. Additionally, a non-zero photocurrent is detected at a bias voltage of 0 V, indicating the presence of an internal built-in electric field and the separation of electron–hole pairs at the WSe$_2$/2DEG interface. This finding suggests the potential for self-powered and self-driven photoelectric detection in this heterojunction. R and D^* are typically used to quantitatively characterize the photoelectric performance of a photodetector. Responsivity is defined as the ratio of photocurrent to incident power density. The formula for responsivity is given as [26]:

$$R = \frac{I_{ph}}{P_{in} \cdot S},\tag{1}$$

where, I_{ph} denotes the photocurrent, P_{in} is the incident light power density, and S is the effective area of light illumination. In this case, the effective area of WSe$_2$/TiO$_2$/2DEG heterojunction is approximately 900 μm^2. The sensitivity of the photodetector, D^* can be determined using the formula [26]:

$$D^* = \frac{R \cdot S^{1/2}}{(2eI_{dark})^{1/2}},\tag{2}$$

where e represents the elementary charge, and I_{dark} corresponds to the dark current. According to the above formulas, the values of R and D^* at different light intensities are calculated and plotted in figure 4(b). As the light power density increases, the photocurrent decreases, causing the R value to decline due to the reduced exciton recombination rate [27]. At the minimum power density of 0.042 mW cm^{-2}, the device achieves its highest values for R and D^*, reaching 0.61 A W^{-1} and 1.1 × 10^{11} Jones, respectively. This indicates that these values are among the highest for photodetectors based on transition metal dichalcogenides (TMDs) [4, 28]. Response time (τ) indicates the speed at which the photodetector responds as the photocurrent rises or decays to a stable level [29]. τ is typically divided into rise time (τ_r) and decay time (τ_d). By calculating the time it takes for the current to increase (or decrease) from 10% to 90% (or from 90% to 10%), the corresponding τ_r and τ_d can be obtained, as shown in figure 4(c). The stable value for τ_r and τ_d are determined to be 70 and 80 ms, respectively. Unlike the
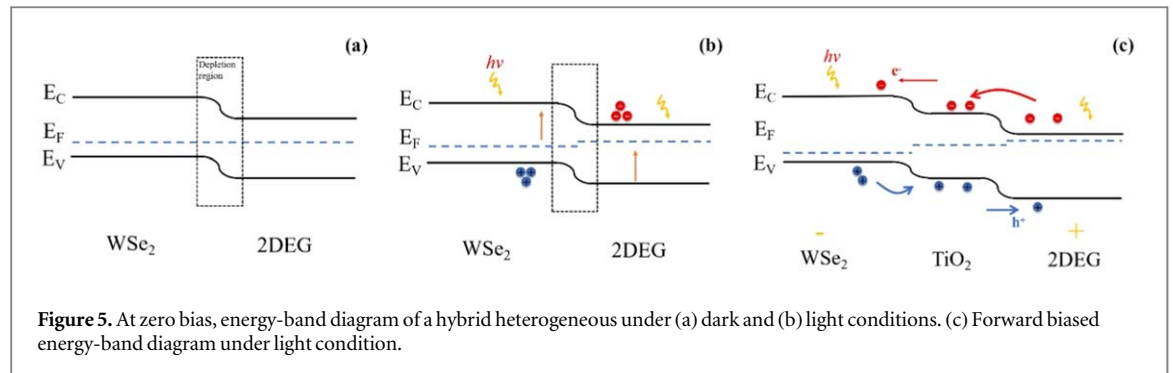
Figure 5. At zero bias, energy-band diagram of a hybrid heterogeneous under (a) dark and (b) light conditions. (c) Forward biased energy-band diagram under light condition.

Table 3. Comparative results in the photosensitivity of two heterojunctions.

Parameter	I_{dark} (nA)	I_{light} ($\times 10^3$ nA)	Switching ratio	Response time (ms)
WSe$_2$/TiO$_2$/2DEG	−5	1.5	105	60
WSe$_2$/2DEG	−35	0.7	30	200

persistent photoconductivity observed in van der Waals heterojunctions (seen in figure 4(d)-(f)) [15], the transient photoconductivity in the hybrid heterojunction is due to the increased photogenerated electron–hole pairs from the buried TiO$_2$ layer, which accelerates their separation. This leads to a significant improvement in the rectification, photoelectric response, and photoresponse time of the hybrid heterojunction, as outlined in table 3.

We aim to analyze the underlying mechanism behind the enhanced photoresponse in the hybrid heterojunction, based on specific energy-band diagrams. The role of the wide-bandgap photosensitive TiO$_2$ layer has been systematically investigated under zero bias and forward bias conditions. And Reactive ion etching of Ar$^+$ affects the barrier height in semiconductor devices, mainly due to changes in the surface stoichiometric ratio, particularly the decrease in oxygen concentration [30]. Etching removes oxygen and introducs oxygen vacancies on the surface, leading to the formation of Ti^{3+} and 2DEG on the surface of STO. This process results in n-type electronic conduction at the surface of the STO substrate.

At zero bias, the contact between p-WSe$_2$ and n-2DEG forms a depletion region in the hybrid heterojunction. Figure 5(a) shows the equilibrium band alignment of the hybrid heterojunction in the dark, indicating a type II band alignment. Under illumination, photogenerated electron–hole pairs in the depletion region can be separated by the built-in electric field. Subsequently, electrons are transferred to the p-WSe$_2$ region and collected by the Pt electrode, while holes flow into the n-2DEG region, as illustrated in figure 5(b). Thus, the energy-band configuration at zero bias in the hybrid heterojunction is similar to that in the planar heterojunction.

At forward bias, the buried TiO$_2$ film provides a tunneling channel in the vertical direction, forming a band alignment of p-WSe$_2$/TiO$_2$/n-2DEG, as illustrated in figure 5(c). Thanks to the medium work function of TiO$_2$, the barrier height at the depletion region is further reduced (from 0.9 eV to 0.7 eV), allowing electrons and holes to diffuse more easily through this region. In the dark, the Schottky barriers at the WSe$_2$/TiO$_2$ (0.70 eV) and TiO$_2$/2DEG (0.71 eV) interfaces suppress the dark current, explaining the lower dark current observed in figure 4(a). Under light illumination, photogenerated electron–hole pairs in WSe$_2$ and TiO$_2$ are separated within the TiO$_2$ layer, where free electrons can more readily transfer to the p-WSe$_2$ region [31]. As the power density increases, more photogenerated carriers are excited, leading to an increase in the forward current. This suggests that TiO$_2$ plays a crucial role in efficient charge carrier extraction.

Furthermore, compared to pure planar heterojunctions, the added TiO$_2$ layer provides better control of transparency and refractive index across the spectral range, impacting light absorption and transmission characteristics. This contributes to improved light absorption and photocarrier emission performance in the heterojunction photodetector [32]. Additionally, incorporating TiO$_2$ as the photosensitive layer enhances carrier transport properties in the heterojunction, affecting the quantity of carriers and their mobility across the energy band [33, 34].

4. Conclusion

In summary, we fabricated the WSe$_2$/2DEG interface and included a photosensitive TiO$_2$ thin film to create a hybrid heterojunction. At room temperature, the device exhibits significant current rectification characteristics, with a peak value of 1.5 μA and a photo-dark current switching ratio of up to 10^2. Regarding photodetection, the WSe$_2$/TiO$_2$/2DEG heterojunction displays excellent photoelectric performance at 405 nm, with a responsivity of 0.61 A W^{-1}, a detectivity of 1.1×10^{11} Jones, and millisecond photoresponse times. The introduction of the wide-bandgap photosensitive TiO$_2$ thin film not only extends the wavelength range of heterojunction detection but also optimizes electron emission and carrier transport characteristics, leading to a significant enhancement in the device's photoelectric performance. This approach, which combines a wide-bandgap dielectric layer with a two-dimensional material-based heterojunction, offers a promising pathway for designing and improving high-performance photodetectors in the future.

Acknowledgments

Data availability statement

All data that support the findings of this study are included within the article (and any supplementary files).

ORCID iDs

Run Zhao ⓘ https://orcid.org/0000-0002-3816-8752

References

[1] Wang Q H, Kalantar-Zadeh K, Kis A, Coleman J N and Strano M S 2012 Electronics and optoelectronics of two-dimensional transition metal dichalcogenides *Nat. Nanotechnol.* **7** 699–712

[2] Bhimanapati G R *et al* 2015 Recent advances in two-dimensional materials beyond graphene *ACS Nano* **9** 11509–39

[3] Khan K, Tareen A K, Aslam M, Wang R, Zhang Y, Mahmood A, Ouyang Z, Zhang H and Guo Z 2020 Recent developments in emerging two-dimensional materials and their applications *J. Mater. Chem.* C **8** 387–440

[4] Jiang J, Wen Y, Wang H, Yin L, Cheng R, Liu C, Feng L and He J 2021 Recent advances in 2D materials for photodetectors *Adv. Electron. Mater.* **7** 2001125

[5] Liang Q, Zhang Q, Zhao X, Liu M and Wee A T S 2021 Defect engineering of two-dimensional transition-metal dichalcogenides: applications, challenges, and opportunities *ACS Nano* **15** 2165–81

[6] Cheng J, Wang C, Zou X and Liao L 2019 Recent advances in optoelectronic devices based on 2D materials and their heterostructures *Adv. Opt. Mater.* **7** 1800441

[7] Tan T, Jiang X, Wang C, Yao B and Zhang H 2020 2D material optoelectronics for information functional device applications: status and challenges *Adv. Sci.* **7** 2000058

[8] Rao G *et al* 2019 Two-dimensional heterostructure promoted infrared photodetection devices *InfoMat* **1** 272–88

[9] Long M, Wang P, Fang H and Hu W 2019 Progress, challenges, and opportunities for 2D material based photodetectors *Adv. Funct. Mater.* **29** 1803807

[10] Wu D *et al* 2021 Ultrabroadband and high-detectivity photodetector based on WS$_2$/Ge heterojunction through defect engineering and interface passivation *ACS Nano* **15** 10119–29

[11] Liu Y, Huang Y and Duan X 2019 Van der Waals integration before and beyond two-dimensional materials *Nature* **567** 323–33

[12] Chen Y *et al* 2021 Unipolar barrier photodetectors based on van der Waals heterostructures *Nat. Electron.* **4** 357–63

[13] You W *et al* 2022 Strong interfacial coupling in vertical WSe$_2$/WS$_2$ heterostructure for high performance photodetection *Appl. Phys. Lett.* **120** 181108

[14] Jiang Y *et al* 2021 Coexistence of photoelectric conversion and storage in van der Waals heterojunctions *Phys. Rev. Lett.* **127** 217401

[15] Ma X *et al* 2022 Bias-tunable persistent photoconductivity for photoelectric memory in van der Waals heterojunctions of black phosphorus/2D electron gas on SrTiO$_3$ *Appl. Phys. Lett.* **120** 061107

[16] Jiang Y *et al* 2022 Giant bipolar unidirectional photomagnetoresistance *Proc. Natl Acad. Sci. USA* **119** e2115939119

[17] Shi J, Zhang J, Yang L, Qu M, Qi D-C and Zhang K H L 2021 Wide bandgap oxide semiconductors: from materials physics to optoelectronic devices *Adv. Mater.* **33** 2006230

[18] Tian R, Gan X, Li C, Chen X, Hu S, Gu L, Van Thourhout D, Castellanos-Gomez A, Sun Z and Zhao J 2022 Chip-integrated van der Waals PN heterojunction photodetector with low dark current and high responsivity *Light: Sci. Appl.* **11** 101

[19] Reagor D W and Butko V Y 2005 Highly conductive nanolayers on strontium titanate produced by preferential ion-beam etching *Nat. Mater.* **4** 593–6

[20] Lee S, Gao X, Sohn C, Ha Y, Yoon S, Ok J M, Chisholm M F, Noh T W and Lee H N 2020 Templated epitaxy of TiO$_2$(B) on a perovskite *Appl. Phys. Lett.* **117** 133903

[21] Shekhar H, Solomeshch O, Liraz D and Tessler N 2017 Low dark leakage current in organic planar heterojunction photodiodes *Appl. Phys. Lett.* **111** 223301

[22] Li Z, Li Z, Zuo C and Fang X 2022 Application of nanostructured TiO_2 in UV photodetectors: a review *Adv. Mater.* **34** 2109083

[23] Zhang J, Zhou P, Liu J and Yu J 2014 New understanding of the difference of photocatalytic activity among anatase, rutile and brookite TiO_2 *Phys. Chem. Chem. Phys.* **16** 20382–6

[24] Chen Y, He A, Liu G, Zhao R, Gao J and Jiang Y 2019 A universal method to fabricate p-n or Schottky heterojunctions based on two-dimensional electron gas *Appl. Phys. Lett.* **115** 241603

[25] Zhou X, Li B, Tian X, Jiang Y, Zhao R, Zhao M, Gao J, Xing J, Qiu J and Liu G 2023 High-photoresponsivity heterojunction based on $MoTe_2$/2D electron gas at the $LaAlO_3$/$SrTiO_3$ interface *J. Phys.*D **56** 205304

[26] Ma R-R, Xu D-D, Guan Z, Deng X, Yue F, Huang R, Chen Y, Zhong N, Xiang P-H and Duan C-G 2020 High-speed ultraviolet photodetectors based on 2D layered $CuInP_2S_6$ nanoflakes *Appl. Phys. Lett.* **117** 131102

[27] Pradhan N R, Ludwig J, Lu Z, Rhodes D, Bishop M M, Thirunavukkuarasu K, McGill S A, Smirnov D and Balicas L 2015 High photoresponsivity and short photoresponse times in few-layered WSe_2 transistors *ACS Appl. Mater. Interfaces* **7** 12080–8

[28] Cheng Q *et al* 2020 WSe_2 2D p-type semiconductor-based electronic devices for information technology: design, preparation, and applications *InfoMat* **2** 656–97

[29] Wang F, Zhang T, Xie R, Wang Z and Hu W 2023 How to characterize figures of merit of two-dimensional photodetectors *Nat. Commun.* **14** 2224

[30] Vanalme G M, Meirhaeghe R L V, Cardon F and Daele P V 1997 A ballistic electron emission microscopy (BEEM) study of the barrier height change of Au/n-GaAs Schottky barriers due to reactive ion etching *Semicond. Sci. Technol.* **12** 907

[31] Fang F, Wan Y, Li H, Fang S, Huang F, Zhou B, Jiang K, Tung V, Li L-J and Shi Y 2022 Two-dimensional $Cs_2AgBiBr_6$/WS_2 heterostructure-based photodetector with boosted detectivity via interfacial engineering *ACS Nano* **16** 3985–93

[32] Kurian S, Seo H and Jeon H 2013 Significant enhancement in visible light absorption of TiO_2 nanotube arrays by surface band gap tuning *J. Phys. Chem.*C **117** 16811–9

[33] Lee K-M, Lin W-J, Chen S-H and Wu M-C 2020 Control of TiO_2 electron transport layer properties to enhance perovskite photovoltaics performance and stability *Org. Electron.* **77** 105406

[34] Kim D, Ghicov A, Albu S P and Schmuki P 2008 Bamboo-Type TiO_2 Nanotubes: improved conversion efficiency in dye-sensitized solar cells *J. Am. Chem. Soc.* **130** 16454–5